Experimental verification of phase modulation and parametric decay from close frequency cavity modes in a multimode microwave ion source

C. Mallick[1,2,a], M. Bandyopadhyay[1,2,a], and R. Kumar[1,2]

[1]Institute for Plasma Research (IPR), Gandhinagar, Gujarat – 382428, India
[2]Homi Bhabha National Institute (HBNI), Anushaktinagar, Mumbai, Maharastra-400094, India

[a)]E-mail: chinmoyju1990@gmail.com;mainak@ipr.res.in

Abstract

Multiple cavity resonant mode excitations in the cavity of an experimental microwave ion sourceare observed. Their interactions within its plasma areimportant aspects that can controlthe microwave (MW) coupling to the plasma as well as the uniformity of the plasma density and its oscillations. The superposition of those close frequency cavity resonant modes, recognized as phase modulation leads to modulate the phase difference between pairs of modes temporally,and thus a new range of the plasma oscillations at the same modulation frequency are recorded.The phase modulation is verified from the signatures of experimentally measured frequency emission from the plasma in an MW ion source cavity and the hot electron population build-up. The increase of the hot-electron populationiscaused by the plasma resonance with the modulated wave.The experimental observations arefurther supported by analytical calculationand by MW-plasma simulation,carried out by a Finite Element Method (FEM) using COMSOL Multi-physics software. Furthermore, the parametric decay (PD)phenomenon of those resonant modes is also responsible for generating ion waves even in theoverdense plasma and thus causes additional plasma fluctuations of the corresponding frequencies. Ion wave contains broadband ion plasma mode and narrowband ion-acoustic (IAWs) wave. The IAWs dominate compared to the ion plasma modes at higher plasma density and are Landau damped by the effective number of ion particles with the increase in the MW power. This paper demonstrates the phase modulation and PD phenomena, those are caused by the excitation of different close frequency cavity modes around the launched microwave (MW) frequency, 2.45 GHz.

Keywords:Microwave ion source, multimode, phase modulation, hot electron, parametric decay, frequency emission of plasma

1. Introduction

Generation of a high density and uniform plasma across a large plasma column dimension are some of the key requirements in the fields of high current microwave ion sources, circular wafer processing technologies, surface plasmon resonance sensors, and antennae applications,*etc*. [1-3]. Better plasma uniformity is achieved by injecting dual-frequency microwaves and/or modulated microwaves in the plasma cavity. The microwave discharge ion source (MDIS) is required to produce a highly intense, singlecharge-state, low emittance, and stable ion beam for utilizing the expected performances of the accelerators operating in large beam loading conditions [4]. To date, several experiments are performed worldwide and demonstrate that plasma non-uniformity and turbulence,*etc*. inside the ion source plasma limit the performance of the accelerators in terms of ion flux reduction, beam halo formation, parametric instabilities, and beam oscillations leading to transverse emittance growth [4-6].The plasma uniformity in MDIS can be achieved by adopting a microwave discharge cavity having multiple cavity resonant modes [1-2].In this case, cavity resonant modes are agitated selectively by injecting variable frequency microwaves (MWs)or modulating the temporal phase difference between the injected MWs which helps to rotate the plasma and increase the diameter of the uniform plasma column [1-3]. Recently, two close-frequency heating (TCFH) experimentsare performed [7] to damp the kinetic plasma instabilities alongside producing anintense and higher charge state ion beam.

The superposition of two close-frequency cavity modes generates a low-frequency wave. The co-existence of thislow-frequency wave in the same interface region modulates the phase of the resultant cavity mode field temporally.This low-frequency modulation (or phase modulation) induces pulsation in the cavity mode field and hence plasma oscillates with the same modulation frequency. The signature of phase modulation in overdense plasma condition isevidenced by its measured frequencyemitted from the plasma.The presence of hot-electron population build-up inside the overdense plasma is due to the modulated wave resonance and the parametric decay effect. The

resonance of the phase-modulated wave with the local plasma electrons occurs near the plasma boundary. Whereas, the parametric decay phenomenon of the cavity modes presents in the dense core of the plasma. It is to be noted that the electron cyclotron resonance (ECR) condition for the launched frequency is not fulfilled near the overdense plasma boundary.

Considering similar experimental configuration and operating conditions, the phase modulation and hot electron generation are supported by a mathematical derivation and also by a microwave plasma simulation carried out by COMSOL Multi-physics software [8-9].

With the increase of the launched microwave power, few cavity modes exceed their corresponding parametric decay (PD) thresholds as their corresponding electric field increase inside the multimode ion source cavity. The parametric decay of the cavity modes produces sidebands around their respective frequencies. The sidebands are captured in the measured frequency emission spectra of the plasma.Similar parametrically generated sidebands were also been observed in fusion machines [10].In the present MDIS, three distinct cavity modes are detected in the frequency emission spectra during plasma operation. By selective coupling of these cavity modes at a particular plasma loading, the plasma density and its uniformity and the structure throughout the volume can be controlled [1-2, 11]. In a similar MW discharge cavity, Cortazer*et al* [11] took images of eight different types of plasma distribution patternsusing an ultrafast imaging technique.He showed that the magnetic field topology and its strength determine the transitions from one plasma pattern to another. The influence of neutral gas pressure and microwave power is insignificant.

It is also found from the existing measurement setup that the PD effect on the cavity modes generates ion type waves [12-16] which are of two types: the ion plasma mode and ion-acoustic wave (IAW).At higher plasma density, IAW dominates compared to the ion plasma modes.At higher launch microwave power, the IAWs disappear. The phase velocities of IAW waves become comparable to the average ion velocity and hence are Landau damped by the effective number of ion particles.

This paper presents experimental verification of temporal phase modulation of the cavity resonant modes excited in the overdense plasma of an MDIS. These resonant modes are closely spaced around the launched 2.45GHz frequency. They are confined near the plasma-sheath interface within a distance of approximately equal to the skin depth under an overdense plasma state [17-22].The paper is organized in the following manner. Sec. 2 describes the theoretical analysis to interpretthe phase modulation and PD phenomenon with the help of analytics and MW-plasma simulation. Then, the experimental methods and their results mainly on the phase modulation and parametric decay phenomenon of multiple cavity resonant modes are discussed in Sec.4 and Sec. 5, respectively. Sec. 5 gives a detailed discussion on the experimental results. Finally, conclusions are drawn in Sec.6.

2. Theoretical analysis

Before presenting the measured frequency-emission spectra and illustrating the phase modulation and the PD phenomena, associated with the cavity modes, the method of multiple cavity modes generation in the absence of plasma is described.The fundamental physical mechanisms of these two phenomena in presence of the plasma are also discussed below with the help of the microwave plasma simulation results [23-25].

2.1 Generation of multiple cavity modes within acavity

Generally, in a microwave ion beam source, the launched microwave wavelength lies within the comparable range of the ion source cavity dimension. Hence, the microwave electric field after entering the cavity becomes a guided wave and is distributed throughout the cavity volume following the pattern of a particular cavity-resonant mode (s), where the power of launched MW is shared. In the present MDIS ion source, multiple cavity modes are excited or altered by modifying the cavity dimensions as well as launching geometry. As mentioned above, microwave launchers, as well as the cavity dimensions, are very critical to electric field distribution inside the cavity, coupled with external magnetic field distributions which control the plasma production. Multiple cavity modes are excited by tailoring the microwave launcher geometry and the cavity dimensions. The details of the microwave launcher and the cavity dimension are discussed in Sec. 4.

The cavity modes of the integrated experimental setup without the plasma condition are identified through microwave simulation. It shows that a significant amount of the microwave electric field exists throughout the cavity volume around the launch frequency, 2.45 GHz. The microwave simulation is performed using commercial COMSOL Multiphysics software considering the simulation geometry as similar to the integrated experimental setup. The simulation calculates the electric field strength in the *r-φ* and *r-z* planes.The cylindrical *r-φ-z* coordinate system represents the radial, azimuthal and axial dimensions. Eight different cavity modes,close to the fundamental cavity mode frequency, 2.45 GHz are found to have significant fraction of power within the cavity. These modes are of TE_{111} type. From the simulation, it is observed that the electric field corresponding to the three cavity modes (②, ③, and ④ in Table-1) has more intensity than the other cavity modes within the cavity. The electric field intensity for these three

cavity modes varies from 55-100 kV/m in the central cavity region. On the other hand, the electric field intensity (~10kV/m) for the other cavity modes at that location is 5-10 times less than those three cavity modes.

2.2 Phase modulation of cavity modes in overdense plasma

Fig. 1(a) shows schematically iso-density contours of simulated plasma along with the electron cyclotron resonance layers. Microwave plasma modeling description is given in [8]. Simulation is performed considering similar experimental configuration and operating environment using COMSOL Multiphysics software [26]. Fig. 1(a) also shows a schematic representation of modulation and PD among three resonant modes (*e.g.*, mode #1, #2, and #3), highlighting the necessary conditions.The superposition of two close frequency modes (#1 and #2 in fig.1a) with some phase delay between them results in a modulated wave [1, 2]. For example, a mode #1 having an axial B-field (H_z) component at some point on cylindrical axis (r, θ, z) can be written using Bessel's function as [1, 2],

$$H_z^{mode\ \#1} = H_0 J_1(Kr)\cos(\omega_1 t)\cos\theta\cos\beta z \ . \quad (1)$$

The eq. (1) is divided by $H_0 J_1(Kr)\cos\theta\cos\beta z$ which gives its normalized form.

$$B_z^{\#1} = A_1\cos(\omega_1 t) \ . \quad (2)$$

Similarly, the axial B-field normalized of mode #2 having an arbitrary phase delay $\emptyset$ with respect to mode #1 can be written as,

$$B_z^{\#2} = A_2\cos(\omega_2 t - \emptyset) \ . \quad (3)$$

The superposition of two modes considering their equal amplitudes ($A_1 = A_2 = A$) gives,

$$B = B_z^{\#1} + B_z^{\#2} = \mathrm{A}[\cos(\omega_1 t) + \cos(\omega_2 t - \emptyset)] \ . \quad (4)$$

Considering, $\omega_2 - \omega_1 = \omega_{LF}$ and since, $\omega_{LF} \ll \omega_1 \& \omega_2$; the eq.(4) can be simplified by letting, $\omega_1 = \omega_2 = \omega$, as

$$B = C\cos(\omega_2 t + \psi)] \ . \quad (5)$$

Here, $\psi = (\omega_{LF} t + \emptyset)/2\,; C = \pm 2\cos\emptyset\cos(\omega_{LF} t - \emptyset)/2.$

To quantify this modulated wave frequencyanalytically, the set of Maxwell's equations are simplified to modified Bessel's differential equations in terms of the H_z [19-21].

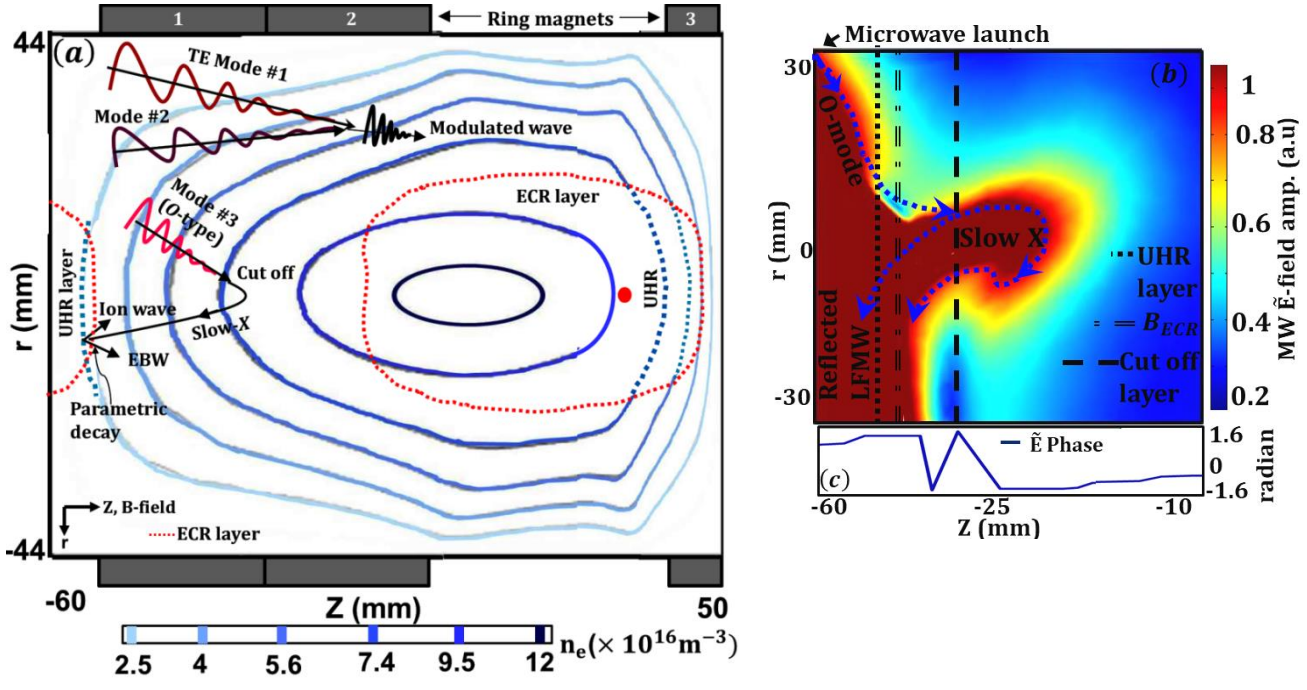

Figure 1: (a) Schematic representation of phase modulation and parametric decay among resonant modes in plasma. Contours show different density iso-surfaces at a particular plasma loading (130 W and 2×10^{-3}mbar) along with showing ECR and upper hybrid resonance (UHR) layer inside the cavity(b) Propagation and mode conversion of MW $\tilde{E}$-field corresponding to an Ordinary (O) type resonant mode (c) Phase angle ($\approx tan^{-1}(Im\,(\tilde{E})/Re\,(\tilde{E}))$of MW $\tilde{E}$-field.

The solution to this differential equation at the plasma-wall interface is: $H_z = A_1 I_m(Kr)$. Here $K^2 = (\omega/c)^2(\varepsilon_2^2 - \varepsilon_1^2)\varepsilon_1^{-1}$and $\kappa^2=(\omega/c)^2\varepsilon_s$. The terms, A_i (i = 1 and 2), K^{-1}, $J_m(\kappa r)$ and $N_m(\kappa r)$, $\varepsilon_i(i = 1 \text{ and } 2)$, ε_s, ω and c are real constants, the penetration depth of MW into plasma, Bessel function of 1st kind, Bessel function of 2nd kind, two components of permittivity present in an MW ($\varepsilon_1 = 1 - \Omega_\alpha^2/(\omega^2 - \omega_\alpha^2), \varepsilon_2 = -\Omega_\alpha^2\omega_\alpha/\omega(\omega^2 - \omega_\alpha^2)$)plasma cavity [19-21], the permittivity of the sheath, wave frequency, speed of light, respectively. Here, Ω_α and $\omega_\alpha$are the plasma and cyclotron frequencies of plasma particle species α (α = i for ion and e for electrons). The condition $K^2 > 0$ determines the possible frequency ranges at which the wavepropagates at the interface region of the plasma-boundary wall. The solution to this inequality gives two frequency ranges which are $\omega_{LF} < \omega < |\omega_e|$and $|\omega_e| < \omega < \omega_1 - |\omega_e|$ respectively. HereLF stands for low frequency and$\omega_{LF}(= 2\pi f_{LF})$ falls in the lower hybrid(LH) frequency range ω_{LH} and it can be estimated as, $\omega_{LH} = [\Omega_i^{-2} + (\omega_i|\omega_e|)^{-1}]^{-1/2}$ and $\omega_1 = 0.5\omega_e + [\Omega_e^2 + 0.25\,\omega_e^2]^{1/2}$. For some typical simulated plasma parameters, *i.e.*, (see Fig.1a), n_i= $5.5\times 10^{15} m^{-3}$,$B = 0.23T$ near the plasma boundary wall, a typical modulated wave frequency is estimated which can be supported for propagation near the plasma sheath. The estimated modulated wave frequency is ω_{LF} = ~1.3 MHz.The eq. (5) shows the phase of resultant axial B-field ψ is modulated with frequency, ω_{LF}. Similarly, the phase of the resultant electric field is also modulated at ω_{LF} [21, 22]. Hence, the force exerted on the electrons by the resultant electric field of the modulated wave where plasma resonance conditions, *i.e.*, $\omega \gg \omega_{pe}$ and $\omega_{pe} = \omega_{LF}$[21, 22] are satisfied, is given by the following function,

$$f_{avg}(t) = \omega_{LF} * (e^2/2m_e\omega^2)\,\nabla(E^2(r - \omega_{LF}t)) \,. \qquad (6)$$

This force is calculated by using simulated results shown in fig.2. Fig.2 (b) gives a radial variation of $\nabla(E^2)_r$ within the plasma sheath thickness (fig.2a).

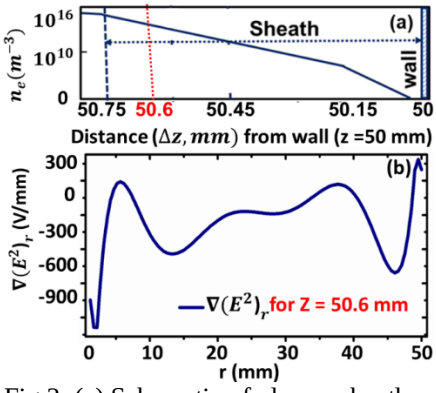

Fig.2: (a) Schematic of plasma sheath near wall (z = 50 mm). (b) Radial gradient ($\nabla(E^2)_r$) of the strongly inhomogeneous electric field within the plasma sheath.

The force using eq. (6) is estimated as $6 \times 10^{-16} N$ for some typical estimated parameters, such as $f_{LF} = 1.3\,MHz$ and $\nabla(E^2)_r$= 1200 kV/m (fig.2). The electron acceleration viaplasma resonance due to this force raises the electron temperature to a very high value near the plasma boundary [27]. Analytical estimation using the present simulated strongly inhomogeneous electric field data suggests that electron temperature may rise to ~ 40keV. The experimental pieces of evidence of the modulated wave and the signatures of hot electron production are presented in Sec. 4.

2.3 Parametric decay (PD)

To explain PD, schematic representation of mode #3 in fig. 1(a) is used. Mode #3 propagating from the high B-field side ($B > B_{ECR}$), which can be oblique w.r.t the B-field and so it may have two components such as extraordinary (X) and ordinary (O) mode. It crosses the ECR layer after reflecting off the cut-off layer and propagates towards the UHR zone ($n_e < n_{critical}$ and $B < B_{ECR}$) [9-12]. As per the literature, the mode conversion (MC) layer exists close to the UHR layer [28] where EM waves are converted into electrostatic (ES) waves through a mode conversion process [12, 29]. The PD phenomenon is likely to occur near the MC layer where the cavity mode electric field ($\tilde{E}$) amplitude exceeds the PD threshold [29, 30]. According to Podoba Y.Y et al [30] the$\tilde{E}$-field's amplitude increases near the UHR layer and also its phase jumps in the mode conversion region. In a similar way, simulation results are shown in figs. 1(b-c) to confirm the existence of the MC layer in MDIS. The figure is interpreted as follows.

In the case of O-mode propagation, fig.1 (b) shows that the simulated MW $\tilde{E}$-field is partly getting reflected at its cut-off layer and converted into a slow-X-mode. This mode conversion (O to slow-X) is verified from the phase of $\tilde{E}$-field (fig.1c). A phase jump (fig.1c) of ~ 3.14radian near the UHR zone confirms the existence of the MC layer [30].The generated slow-X mode is unable to penetrate the overdense plasma region and hence is reflected. Fig. 1(b) evidences a bending in slow-X mode's propagation due to its reflection from over-dense plasma and hence it reaches the UHR layer. As a result, the amplitude of $\tilde{E}$-field corresponding to the slow-X mode MW is increased near the UHR layer and may cross the PDI threshold value. As per the literature survey [12, 28-30], the PDI may generate an electron Bernstein wave (EBW) and ion wave through the 'O-X-B' mode conversion process. The generated ion wave is seen as a sideband of different resonant modes in the measured frequency emission spectra from the plasma and is discussed in sec.4.

On the other hand, considering the$X$-mode component of the cavity resonant mode, a directconversionof X – mode into an EBW and ion wave occurs near the UHR layer [12] through

the *'X-B'* conversionprocess. The PD-created EBW is not detectable through an electrostatic Langmuir probe [12]. Hence ion waves are only visible in the sidebands of resonant modes observed in the measured emission spectra and are considered as the signature of the PD phenomenon.The ion waves do not see any density cut-off and hence are damped out due to interactions with ions, discussed in sec.4.

In the PD process, the excited cavity modes are used to decay into two daughter waves. The frequencies (f_1 and f_2) of both the daughter waves are lower than that of the parent (or cavity, f_0) mode and follow the relation $f_2 = f_0 - f_1$. The parent wave may interact non-linearly with any one of the generated daughter waves and thus creates the third wave of frequency higher than that of the parent wave ($f_3 = f_0 + f_1$) [12].In overdense plasma, the frequency of resonant mode before and after PD is assumed to be equal because their difference lies only in the order of few hundreds of kHz [15]. The PD processfollow the frequency and k-vector selection rules [12], *i.e.*,

$$f_2 = f_0 - f_1; f_3 = f_0 + f_1 \quad (7)$$

$$\text{and } k_2 = k_0 - k_1; k_3 = k_0 + k_1. \quad (8)$$

Here, f_0/k_0, f_1/k_1 and f_2/k_2 are frequencies/k-vectors of cavity resonant modes ($f_{\#i}; i = 1,2, \dots etc.$), corresponding daughter wave ($f_{\#i} - nf_{ion}$) and nf_{ion} respectively. Here, $n = 1,2$ .... etc. From experimental data, it is found that the measured *k*-vectors follow the selection rules whose values are given in Sec.4. The sideband *k*-vector (k_1) is very close to that of cavity mode k_0. The k-vectors k_0 and k_1 are small compared to k_2. Here the measured *k*-vector by the Langmuir probe is actually k_2 ($\approx \sqrt{(k_{\parallel}^2 + k_{\perp}^2} = k_{ion}$) and used in the k-vector selection rule. Here, k_{ion} denotes the k-vector of PD created ion wave of frequency, f_{ion}.However, the rate for parametric decay (PD) of these cavity modes strongly increases if the cavity mode frequencies become very close to launched MW frequency under a particular plasma column dimension [17,18].

2.4 Classification of ion wavesand their damping

The PD-generated ion waves are recognized by the dispersion eq.(9) [31]. In the present magnetized plasma source, the electron mass is smaller than the ion mass ($m_e \ll m_i$). For 5eV electron temperature and density ~$10^{17} m^{-3}$, the ion wave speed and Debye length (λ_D) in plasma are estimated as ~2.3×10^4 ms^{-1} and ~3×10^{-5} m, respectively. By measuringthe k-vector of ion waves (k_{ion}) ~$245 m^{-1}$, it is found that $k_{ion}\lambda_D \ll 1$ condition[9, 15] is satisfied for applying eq. (9) to classify the ion waves. Hence, the dispersion relation for ion wave can be written as [31],

$$\omega_{ion}^4 - (\Omega_i^2 + k_{ion}^2 c_s^2)\omega_{ion}^2 + \Omega_i^2 k_{ion}^2 c_s^2 \cos^2\theta = 0 \quad (9)$$

Here, Ω_i, c_s and θ are the ion gyro frequency, ion wave speed, and angle of MW propagation direction *w.r.t.*theapplied B-field orientation respectively. Considering the reverse direction of MW propagation after PD [15, 32] and correspondingly using the k-vector selection rulek_{ion} can be approximated as $k_{ion} \cong 2k_0 = k_2$ [15, 31]. Considering this approximation, eq. (9) gives solutions of the ion wave frequencies, as shown in eq. (10) [32].

$$\omega_{ion}^2 = \frac{1}{2}(4c_s^2 k_0^2 + \Omega_i^2 \pm (16c_s^4 k_0^4 + \Omega_i^4 - 8c_s^2 k_0^2 \Omega_i^2 \cos 2\theta)^{\frac{1}{2}}). \quad (10)$$

Where '+' sign root represents electrostatic ion cyclotron wave (EICW) and '–'sign root gives IAW wave. The existence of IAWs is only demonstrated in the current paper and EICW investigation is under study.The phase velocity of IAWs can be written as, $\frac{\omega_{IAW}}{k_{ion}} = \{k_B(T_e + \gamma_i T_i)/M_i\}^{1/2}$[9], where ω_{IAW}, k_B, γ_i,k_B, T_i, and M are the IAW frequency, *k*-vector, one-dimensional ion compressionconstant, Boltzmann constant, ion temperature, and ion mass, respectively.To recognize the PD generated IAWs, the corresponding *k*-vectors ($k_{\perp}$and $k_{\parallel}$) are estimated from the measured Langmuir probe data. In the present MDIS cavity, IAW appears for $k_{\parallel}$ values typically in the range from 7 to 22 m^{-1} and$k_{\perp}$ varies from ~245 to 250 m^{-1}. Putting measured *k*-vector and Ω_i= 55 kHz (radial position, r = 5 mm and B = 0.05 T) into eq. (10), the IAW frequency is estimated within the range of measured sideband frequencies, discussed in sec.4.

The generated IAWs can be damped through the electron-electron collisions under certainconditions which are discussed in detail by Bychenkov V. Y et al. [33]. He also discusses the ion contribution to the ion-acoustic wave damping process.The applicable conditions are: ion temperature is low (or comparable) compared to that of the electron temperature under the presence of a weak microwave electric field, and the wavelength limit (i.e.,$k_{ion}\lambda_{De} \leq 1$). From the dispersion relation presented in the ref [15],frequency that covers the whole range of ion oscillations (f_{ion}), the ion-acoustic wave frequency in the limit of $k_{ion}\lambda_{De} < 1$, is written as, $f_{IAW} = f_{pi}(k_{ion}\lambda_{De})$. Considering the measured $k_{ion}\lambda_{De}$ values, the f_{ion} also ranges in between 238 kHz to 873 kHz,as observed in the measurement of the frequency emission from the overdense plasma.The first condition indicates that the phase velocity of IAWs is comparable to the ion thermal velocity. Due to this, the interactions between the IAWs and ions happen and hence the ions can be decelerated by the Landau damping mechanism like electrons, the ion temperature is getting decreasedand the electron temperature is being increased where the Landau damping occurs. As a consequence, the electron energy distribution is affected which is discussed in Sec. 5 with the use of the measurement data.

3. Experimental Method

A schematic view of MDIS and its plasma diagnostic setup is shown in fig.3 [8]. Fig.3 shows four ring magnets (1.38 T each, magnetization is along with the thickness) surround the plasma chamber co-axially in mirror-B configuration mode. In this experiment, right-hand polarized MW (*R*-wave) of frequency 2.45 GHz is launched using a microwave launcher to the cavity from the high B-field side of one set of the permanent ring magnet [8-9]. The launcher geometry includes a four-step ridge waveguide and a high voltage (DC) break cum vacuum window that connects the cavity. For ion beam extraction purposes, the launcher unit and the cavity are integrated with a vacuum chamber through an aperture having adimension of few millimeters. The vacuum chamber houses a three-grid ion extraction system and the beam emittance diagnostic setup. A boron nitride (BN) plate is placed at the inner plasma-facing side of the plasma-grid surface to get a higher extracted ion current density [16].The description of the setup is shown in fig.3.However, it is to be noted that the present experimental setup is working on the ion source with magnetic mirror field configuration and not using the sextuple/octupole magnetic field configuration, normally used in ECR ion sources.

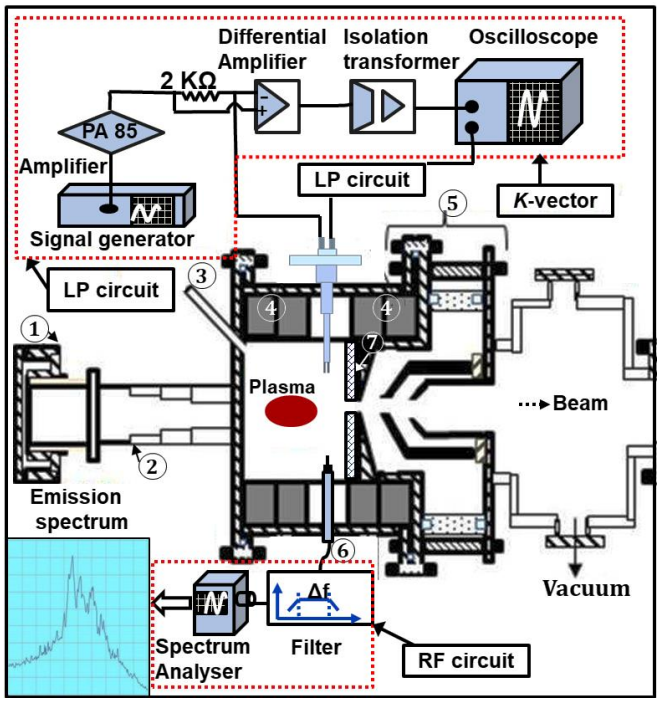

Figure 3: Schematic of plasma diagnostics setup of MDIS. ① HV break and vacuum window; ②Four step ridge guide;③ Gas inlet;④ Ring magnet pairs;⑤ ion extraction grids;⑥ RF probe;⑦ Boron nitride (BN) plate.

If the launched MW is exactly parallel to the B-field axis, it is capable to propagate towards the dense plasma region. However, due to the mirror field configuration in the present setup, the MW axis does not exactly coincide with the magnetic axis. As a result, both the Extraordinary (*X*) mode and the Ordinary (*O*) mode would exist in the plasma irrespective of launching a pure *R*-wave. The breakdown of nitrogen gas in a vacuum is done by injecting MW power (set-power) from 50W to 700W. The reflection of MW power from the plasma ranges between 5% to 10% with the increase in set-power [8]. A more detailed description of the experimental setup and the diagnostic methods can be found in [8].

During the experimental campaign, the frequency emission spectra from plasma are measured by a probe tip (also denoted as RF probe).The probe tip is placed near the beam extraction grid location (r, z = 0, 25 mm), as shown in fig.3.The probe detects frequency emission from the cavity with and without plasma. The frequency signal collected by the probe is analyzed using an RF circuitry consisting of a microwave Spectrum Analyser (SA)(model: FSH8, make: ROHDE & SCHWARZ, band: 100 Hz-8 GHz)and FSH4View data acquisition software. A band-pass filter(LORCH MICROWAVE make, model: 9IZ3-2500/A1000-S) is employed to select a particular frequency band around 2.45 GHz.Despite launching 2.45 GHz MW ($\omega_0 = 2\pi f_0$), (bandwidth ~10 - 25 MHz [8]), different cavity resonant modes with and without plasma are observed inside the cavity around 2.45 GHz. The Sairemcompany-made microwave generator is tested separately with low power operation on a test bench to ensure only a single peak of pump frequency at ~ 2.43 GHz.

The chamber is maintained at base pressure ~ 1×10^{-7} mbar and the observed frequencyemission reported here are in the operating pressure range of $2 \times 10^{-4} - 1 \times 10^{-3}$ mbar [8].The floating potentials of plasma are recorded by a two-tip-based Langmuir probe.Two tips are used as two independent Langmuir probes as shown in fig. 3. Time-varying floating potential signalsare separately coming from the two probe tips simultaneously and acquired by an oscilloscope. The phase difference of the floating potential of each probe divided by their separation measures the wavenumber k [8]. The k-vector of a plasma wave is constructed by aligning the plane of the two probes in the perpendicular (denoted as $k_\perp$) as well as parallel (symbolized by $k_\parallel$) direction with respect to the B-field.

4. Experimental results

As discussed before, the frequency emission from the plasma is recorded by an RF probe for different set-powers. In the beginning, spectrum in vacuum condition is obtained to record the presence of different cavity resonant modes (also called vacuum cavity modes (VCMs)) inside the ion source cavity [9], to understand the basic characteristics of the geometry. The VCMs are given in Table-I [9]. With

increasing the set power, the plasma moves from underdense condition to overdense condition. The transition starts from 130W. During plasma discharge, modified characteristics of the frequency spectra are shown in fig.4 (a) and also noted in Table-1 for 180W (over-dense condition) case.

To understand the frequency shift in presence of plasma, the plasma is assumed to be collisionless. Under this assumption, the shift is calculated from relation, $f_{nml}^{TE} = [(\frac{f_{pe}}{2\pi})^2 + (\frac{c}{2\pi})^2\{r_{nm}^2 + (\frac{l\pi}{d})^2\}]^{1/2}$ [23-26]. The terms, f_{nml}^{TE} are resonant mode frequencies in presence of plasma having a 3D field pattern, characterized by an integer, n (≥ 0), m (> 0), and l (≥ 0). Here, f_{pe}, c, d, a, and p'_{nm} ($\equiv r_{nm} \times a$ for $TE_{n=1,m=1,l=1}$ modes) are electron plasma frequency, speed of light, chamber length, radius, and m^{th} root of the first derivative of n^{th}-order Bessel function, respectively. For 180 W, the frequency shift is estimated as ~65 MHz, which is consistent with the measured frequency spectral shift (Table-1 and fig.4a).In fig.4(a), the lower side peak of each excited cavity mode represents electron plasma frequency (f_{pe}) which isjustified in Sec.5 below [15]. The difference between each excited mode (*i.e.*,$f_{\#i}, i = 1,2, \ldots$) and its corresponding first lower side peaks (*i.e.*,$f_{\#i} - f_{pei} = f_{pij}; i,j = 1,2, \ldots$) give ion plasma mode (*i.e.*, $f_{pij}; j = 1,2, \ldots$) and is discussed in Sec.5.

Fig.4 (a) shows only fundamental f_{pi}in the low-frequency region of the emission spectra at 130 W set power. Whereas, at 180W, both $f_{pi}$and it's first harmonic are present side by side in the spectra. Harmonics of f_{pi} are not visible in low power.This is because of the low intensity of the interacting modes for 130W (25 dB down relative to 180W case).

Table-1: Vacuum cavity and excited cavity (in presence of plasma) resonant modes measured at 180 W and 1.5×10^{-4} mbar (fig.4a). All modes are TE_{111} type [9].

Vacuum resonant mode frequencies (GHz) & peak no.	Excited cavity mode frequency (GHz) & peak no.	Normalized intensity *w.r.t* f_0 (Vacuum and excited mode)
2.295& ①	2.36 & #1	0.28 and 1.1
2.378 &②	2.449 and #2	0.579 and 2.75
2.421 &③	Not appeared	0.64 and 0
2.456 (f_0)&④	2.529 and #3	1 and 2
2.539 &⑤	2.604 and #4	0.37 and 0.8
2.568 &⑥	Not appeared	0.38 and 0
2.622&⑦	Not appeared	0.32 and 0
2.691 &⑧	Not appeared	0.27 and 0

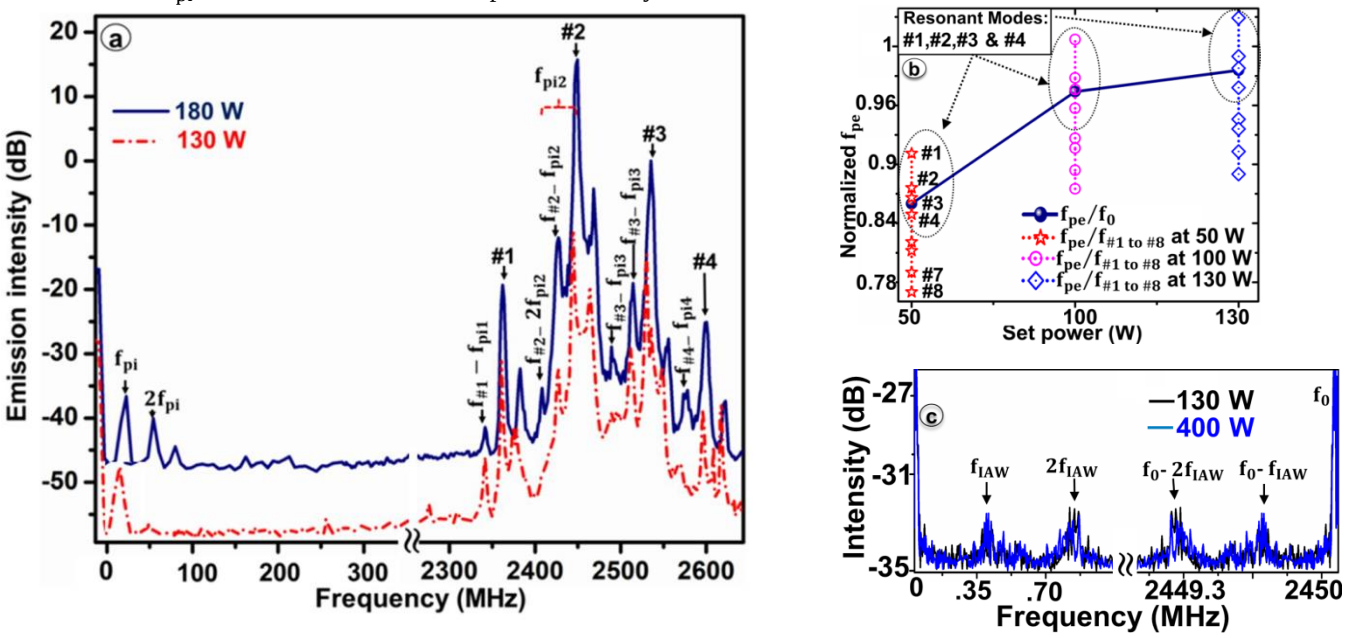

Figure 4: (a) Frequency emission spectra showing parametric decay among cavity modes. The resolution bandwidth of 100 kHz is taken during the measurement. The spectrum is taken at differentset-powers and 2×10^{-4} mbar pressure. (b)Variation of normalized $f_{pe}$with different set-powers highlights propagating modes eligible for PD. (c) Emission spectrum indicates PD of excited cavity mode, 2.45 GHz at different set-powers.

Fig.4 (a) also shows the first pair of sideband peaks (lower and upper) is spaced apart by ~20 - 22 MHz from their respective parent resonantmode frequency. The lower sideband peak represents electron plasma frequency f_{pe} as discussed before, is very close to f_0. Here, the ($f_0 - f_{pe}$) values corresponding to ~20-22 MHz, are generated due to the PD phenomenon [15] as the resonant mode obeys the relation, $f_0 \cong f_{pe\_average}$ [15, 32]. It is to be noted that around density $1.5\times 10^{17}\mathrm{m}^{-3}$ (180 W), f_{pi} is also estimated as ~20-22 MHz.

To prove the PD phenomenon, the estimated f_{pe} for different powers is normalized with respect to (*w.r.t.*) the launched frequency f_0 and is shown in fig. 4(b). The normalized values closer to unity but slightly less implies favorable condition for the occurrence of PD [34]. More than unity corresponds to cut-off. Similarly, f_{pe} is again normalized *w.r.t* each of the cavity resonant mode frequencies $(i.e., f_{\#1}, f_{\#2} \ldots etc.)$ separately. The latter quantities are compared with the former normalized ones in fig. 4(b) to understand the decaying cavity modes. Fig. 4(b) shows four modes (#1, #2, #3 and #4) remain close to f_{pe}. Hence, as per the literature [34], the PD thresholds for these modes (#1 to #4), are less compared to other remaining vacuum cavity modes. Hence, the decaying patterns come from three-wave interactions, *i.e.*, the excited cavity resonant mode ion plasma mode and the sideband [15, 33].

The *X*-mode is resonantly absorbed through the PD process near the UHR layer [12, 28-30] as discussed before in sec-3. In fig.4 (b), the mode $f_{\#1}$ is unable to propagate inside the plasma because its frequency is less than f_{pe} for 130W of set power. However, the mode $f_{\#1}$ is still present near the measured plasma boundary location even for 180W set power and shown in fig.4 (a). Possibly, the emission signal is collected when the $f_{\#1}$ mode propagates until meeting the cut-off layer and it is then converted into a slow *X*-wave, and then converted to an IAW. Different cavity resonant modes decay parametrically at different places which would give rise to differentf_{pe}. This would cause the frequency separation between each resonant mode and its corresponding sideband peak to be different even for the same power. Due to that reason, the sideband values corresponding to each resonant mode show different (ranging from 20-22 MHz) in the spectra (Fig.4a). Sideband peaks are represented by different notations for clarity.

Fig.4(c) shows the PD to occur even in highly overdense plasma (>$1.5\times 10^{17}\mathrm{m}^{-3}$ for power > 180W) as the excited cavity modes obey the frequency and *k*-vector matching rules as per experimental observations [9].It generates narrow peaks which are labeled as nf_{IAW} in fig.4(c), represents ion waves ranging from 238 kHz to 873 kHz. Here *n* corresponds to harmonics of IAW.

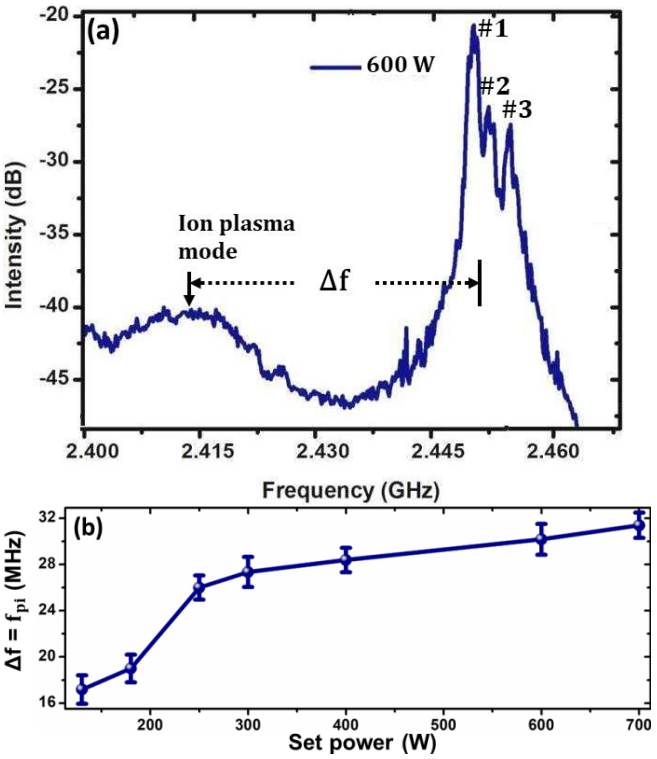

Figure 5: (a) Frequency spectrum at higher set-power with 10kHz bandwidth. Here $f_{pe\_average} \approx 2.41GHz$ and $\Delta f = f_{pi} \approx 31MHz$, (b) Sideband separation (Δf) or ion plasma mode frequency with set-power

It becomes more interesting to understand the existence of cavity resonant modes for higher power > 180W, in which the plasma densities are higher and the peaks corresponding to ion plasma mode would be well separated from the cavity resonant peaks and easy to analyze.

In view of this, a zoomed version of the spectrum near launched frequency (fig.5 (a)) is given. It shows the excitation of three cavity modes at much higher plasma density (>$3\times 10^{17}\mathrm{m}^{-3}$for 600 W set power). Corresponding ion plasma modes (figs.5 (a,b)) which are superposed to form a relatively broad peak corresponding to $f_{pe\text{-}average}$ and are separated by Δf ~ 30-32MHz. In addition, sidebands other than ion plasma modes arise around each excited cavity mode, shown in fig. 5(a). The variation of ion plasma mode frequency for different set power is shown in fig. 5(b). Two regimes are observed in that figure and 250W is the boundary between these two regimes. Explanation of this observation is discussed in the latter part of this section.

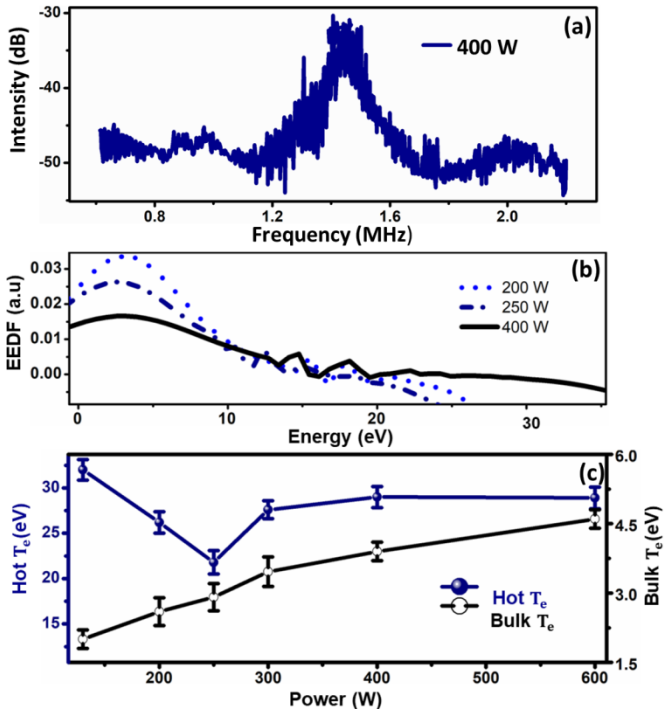

Figure 6: (a) Spectrum acquired by the spectrum analyzer (b) Electron energy distribution function (EEDF) obtained from Langmuir probe data for different set power, (c) Variation of bulk and hot electron temperature (T_e) with set power.

Every resonant cavity peak (fig.5a) is spaced apart from each other by a frequency of ~1.3 MHz, which effectively creates temporal phase modulation of the same frequency [1, 2]. To support this, a signal acquired by a Langmuir probe and a spectrum analyzer combination is shown in fig.6 (a). The same probe is also used to generate electron energy distribution functions (EEDF) for different powers and shown in fig. 6(b). It is observed that with power > 250W hot electron population increases. A relative variation of bulk and hot electron temperature for different set power is shown in fig. 6(c). The phase modulation is considered to be one of the possible reasons for hot electron generation [21-22, 27]. The other phenomenon: parametric decay that can be responsible for high-energy electrons is also referred from the available literature in the discussion section below.

To get a closer view of the parametric decay of those excited cavity modes in over-dense plasma conditions, fig. 5a is further zoomed and a frequency span of ~16 MHz around the 2.45 GHz frequency is plotted in figs. 7(a-c).The spacing between the excited cavity mode (*e.g.,* #2) and its first lower sideband peak (fig.7a), gives the ion-acoustic waves (IAW)because of the PD phenomenon. The PD of resonant mode into ion-acoustic waves in the overdense plasma is the result of the nonlinear coupling of energy between the cavity mode and electrostatic ion acoustic wave.

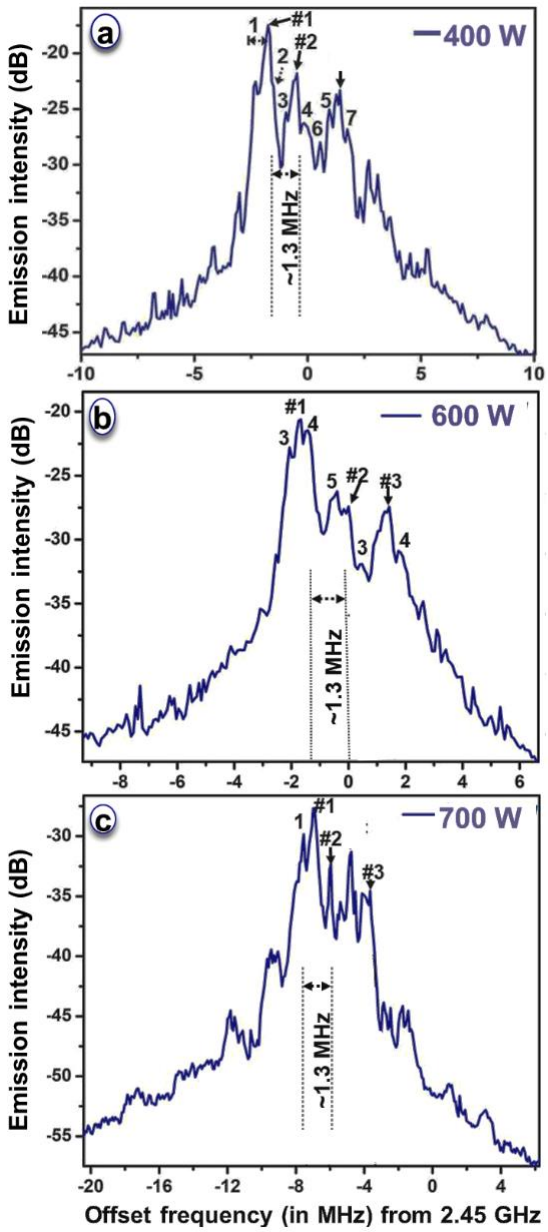

Figure 7: A closer view of emission spectra around 2.45 GHz peak highlighting IAW sidebands (denoted as 1, 2, 3… etc.) around resonant modes for three set powers. The spectra are taken at 6×10^{-5}mbar pressure, 0.06 T B-field and probe position (r, z) = (10 mm, 25 mm). Resolution bandwidth (RBW) and its span are kept at 10 kHz and 10 MHz, respectively. (a) 400 W (b) 600 W and (c) 700 W.

The narrowband peaks (fig.7a) are identified as IAWs from the dispersion [31] using "–ve" root which is given in Sec. 3. Also, the sideband frequencies which correspond to IAW waves are verified from the electron temperature relation of ion-acoustic speed, as clarified in Ref. [9]. The narrow sideband peaks (see figs.7 (a-c)) are numbered as 1 (555 kHz), 2 (238 kHz), 3 (476 kHz), 4 (317 kHz), 5 (397 kHz), 6 (873 kHz and 7 (348 kHz), respectively.

The PD threshold and generation/destruction of IAWs *w.r.t.* the power are clearly visible in figs.7(a-c).Figs.7 (a-c) show that, with further increase in power (*i.e*., 400 W to 700 W), the number of IAW peaks is reduced in the sideband locations due to its damping in overdense plasma which is discussed in detail in Sec.5. Fig. 7(c) clears that, almost all the IAWs, contributed by the three different resonant modes, are damped out completely beyond 700 W, at a much higher plasma density. It can also be visualized in figs.7 (a-c) that the whole spectrum is shifted towards the lower frequency region with the increase in density. This kind of shift (1.2-6 MHz) is resulted from Doppler Effect, as described in [9].

5. Discussion

The observations of ion plasma mode and IAW can also be explained analytically using ALIEV and SILLIN's theory and also by MW electric field simulation using COMSOL Multi-physics software.

It is observed that the low sidebands are ion plasma modes. The separation of the sideband peaks which represents ion plasma mode increases with power as presented before. At higher plasma density (overdense), the sidebands are dominated by IAWs as shown in fig.7(a).The presence of ion plasma mode can be explained by using ALIEV and SLLIN'S theory [15, 33]. They described that ion plasma frequency range can exist if an intense MW $\tilde{E}$-field (*i.e.*, $x \geq \lambda_{De}$) is present in plasma and *k*-vector has a large value ($k_{ion} \approx {\lambda_{De}}^{-1}$). Here, $x\ (= e\tilde{E}/m_e{\omega_0}^2)$ and $\lambda_{De}(\upsilon_{Te}/2\pi f_{pe})$are amplitude of electron oscillation in MW $\tilde{E}$-field and electron Debye length, respectively. Here, MW-plasma simulation shows MW $\tilde{E}$-field varies from 120kV/m to 20kV/m with the increase of density from ~$1\times 10^{16}m^{-3}$ to $1.3\times 10^{17}m^{-3}$for 50W to 150W set power respectively [8, 35]. Hence, the amplitude (x) of electron's oscillation may vary from ~90 μm to 37 μm for the above range of MW $\tilde{E}$-field. On the other hand, the measured data show λ_{De} varying from 50 μm to 36 μm for a fixed thermal electron temperature of 3.5 eV with a density transition from $7.3\times 10^{16}m^{-3}$ (130W) to $1.5\times 10^{17}m^{-3}$ (180W) respectively. It implies MW $\tilde{E}$-field is intense inside the cavity as, $x \geq \lambda_{De}$ and hence the considerationof the sidebands as ion plasma modes is justified for the aforesaid conditions. The frequency, f_{ion}depends on x for a given λ_{De} as per the relation, ${f_{ion}}^2 = {f_{pi}}^2\ (1-\frac{J_0^2(k_{ion}.x)}{1+(k_{ion}{\lambda_{De}}^2)})$ [15]. Moisan*et al* [15, 33] also concluded that IAW can reach f_{pi} even within the region, $k_{ion}\lambda_{De} \leq 1$. Since, $k_{ion}\lambda_{De} \ll 1$ in the present over dense plasma case (see fig.8) for power >180 W, IAW wave is unable to reach f_{pi} range. Hence, IAW modes dominate with the increase in set power (above 180 W) compared to ion plasma mode.

As presented before, above 250 W set power as per experimental observations, another wave oscillation appears which is proved to be a modulated wave generated from the temporal phase difference between cavity resonant modes. The intensity of this modulated wave increases with set power whereas; the IAWs disappear at such higher power (700W). The disappearance of IAWs is attributed to the damping of the mode due to theinteraction of IAW waves with the ion particles.The interaction is possible only if the phase velocity of IAW waves becomes comparable to the average ion velocity [36]. The number of ion particles that are effective for Landau damping increases as the phase velocity of IAW approaches the ion thermal velocity [37] and the supportive calculation is as follows.

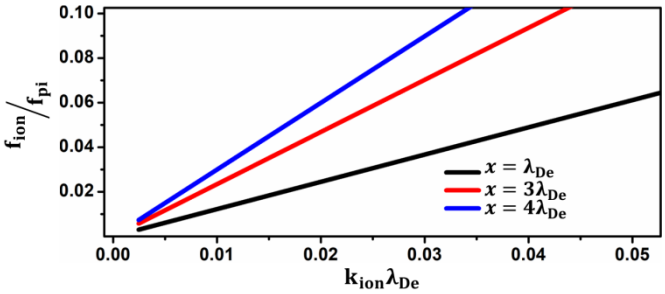

Fig.8: Ion wave dispersion intense MW $\tilde{E}$-field ($x \geq \lambda_{De}$)

For the observed IAW frequency range of 238-873 kHz and measured*k*-vector of value ~ $245m^{-1}$gives the ion-acoustic phase velocity as (6×10^3 – 2×10^4m/s)and correspondingaverage ion temperature T_i is of value ~1 eV [9].The average ion thermal velocity using T_i value is ~2.6×10^3m/s and is found to be comparable to each other. Hence, one can conclude that IAW interactswith the ions and damped due to the Landau damping mechanism[36-38].

Due to this damping, the fine frequency spectrum representing the IAWs, measured under different operating conditions, disappears in the frequency spectrum as shown in figure 7 of the manuscript. It is known that the IAW damping through the ions yields the perturbation in the electron energy distribution function (EEDF) under several inhomogeneous plasma conditions[33].To understandthis, the two Langmuir probe measurements are performed, and their corresponding electron energy distribution functions are compared in fig. 9. Before presenting the measured electron distribution function, it is confirmed before [15] under several conditions that,f_{pi} oscillations are actually IAWs.

In the reference [33], it is discussed that although the electron contribution to the IAW damping dominates in the wavelength limit $k_{ion}\lambda_{De} < 1$, the ion contribution to the IAW damping is also important when the ratio of electron to ion temperature is large (e.g., T_e/T_i>1). It is found that the

temperature gradient in the electron distribution exists if the ion-acoustic wave (IAW) damping is present. In other words, it can be conjectured that the energy from the electrons is transferred to ions through IAW Landau damping. As a result, the ion temperature increases by Landau damping and causes the reduction of electron temperature, and hence a gradient of the electron temperature arises.

The IAW damping rate changes in an inhomogeneous plasma. In the reference [33], it is presented that in the wavelength limit, $k_{ion}\lambda_{De} < 1$, the change in IAW damping rate corresponds to the presence of the unstable ion acoustic wave (IAW). It is proved theoretically in reference [33] that the change in the damping rate is associated with the electron temperature gradient. The electron temperature gradient is captured in the two independent Langmuir probe data as shown in fig.9, placed at two different positions (probe 1: (r,z = 0, 25 mm), probe 2: (r,z = 0, 20 mm)) with same operating conditions. Two different Langmuir probe data showsin fig.9 that the plots representing the distribution function are having different slopes across the electron temperature range, 0 eV to 35 eV. Near the 15 eV to 25 eV range, the perturbation in distribution is observed as shown in fig.9.

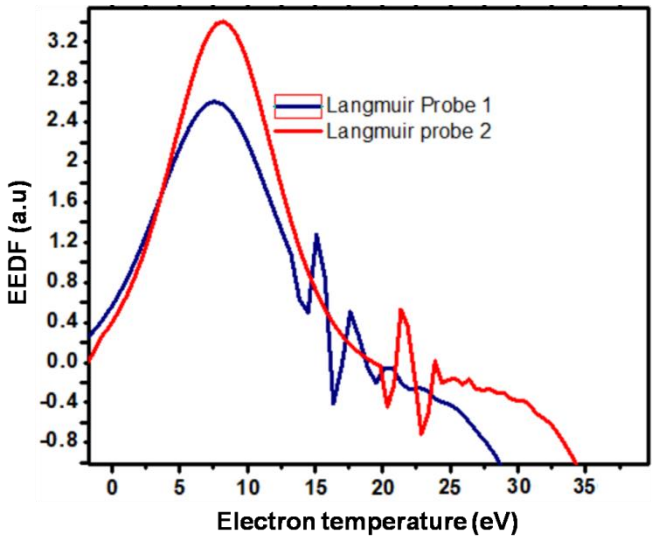

Fig.9: Perturbation in electron energy distribution due to ion-acoustic wave damping through the ions in inhomogeneous plasma. Data is for 400W MW power with 3×10^{-5} mbar pressure.

From the literature survey, it is understood that the PD phenomenon is associated with the generation of electron Bernstein waves (EBWs) along with the IAWs. The EBWs are often depicted as the cause of hot electron generation in magnetized plasmas.So, there is a possibility that the electron Bernstein wave is generated from the parametric decay of the cavity modes in the present plasma source also. However, the existing Langmuir probes are not able to detect the EBWs in the overdense plasma. This is because the EBW wavelength is much shorter than the presently used Langmuir probe tip-length (4 mm) [1].It is known from the literature survey that parametric decay can also generate other types of ion waves, i.e., ion Bernstein waves (IBWs) or Lower Hybrid oscillations (LHOs). However, the studies on the existence of these waves in the present experimental setup are reserved for future work.

6. Conclusion

Temporal phase modulation of the close frequency cavity modes and parametric decay of those cavity modes are observed in the microwave plasma experiment of a multimode ion source. The signatures of the phase modulation and thereby the hot electron generation are also observed experimentally. The modulation frequency is observed from frequency emission from plasma measured by RF circuitry. The hot electron generation is confirmed by Langmuir probes measurement placed near the plasma source boundary.

Considering two close frequency cavity modes with an arbitrary phase delay between them, it is demonstrated by the experimental observations supported with a mathematical derivation that the resultant phase of two superposed cavity mode fields modulates temporally near the boundary of the microwave plasma. The frequency of the modulation is determined analytically. The resonance of the plasma electrons with the modulated wave near the boundary of the plasma builds up the hot electrons near the boundary. The temperature of the hot electrons is estimated analytically and found to vary in the 10's of keV range. To estimate the hot electron temperature analytically, a simulated microwave electric field that is strongly inhomogeneous near the plasma boundary is used. The simulation is performed by COMSOL Multi-physics software assuming computational parameters similar to the experimental configuration and operating environment. It is concluded that the plasma resonance with the modulated wave near the boundary creates a strong inhomogeneous electric field in the sheath and is responsible for the hot electron production.

It is to be noted that the force generated by the phase modulation can produce high-temperature electrons (T_e up to 40 keV) that reaches maximum value near the plasma boundary.Consequently, one should expect hot electrons to be generated at the plasma boundary. However, from several experimental campaigns, it is found that those hot electrons are not restricted near the boundary only but present across the plasma volume due to their mobility. Since the magnetic confinement is poor in the present setup; it is hard to trust that the electrons generated near the walls could fill the whole plasma volume after a back and forth reflection. So, it It seems that,only the phase modulation cannot explain the

hot electron generation as a whole in the plasma but just a portion of it.Parametric decay is another possible candidate in explaining the hot fraction of electrons present in the microwave plasma source volume.

The parametric decay (PD) of the cavity modes in highly inhomogeneous plasma is observed by measuring a wide range of frequencies emitted from MW ion source plasma. In a highly inhomogeneous microwave plasma, the parametric decay of the different cavity modes causes to excite ion plasma waves before and after their respective plasma cut-off density regions. These ion plasma waves approach the ion-acoustic wave (IAW) frequencies under the presence of the intense microwave electric field near the cut-off density locations of those cavity modes.The plasma is overdense in those locations. The conclusion on the ion-acoustic wave propagation is verified from the measured frequency emission from the plasma.The *k*-vector measurements are performed using the two Langmuir probes diagnostics placed near the microwave plasma boundary.The frequency emission from the plasma shows fine structures of the cavity modes and the ion plasma waves contain useful pieces of information on the microwave power absorption by the plasma. It is found that the undamped ion plasma waves in the highly inhomogeneous plasma exhibit fine structure in the frequency emission spectra. The ion-acoustic waves that are damped in the plasma disappear in the frequency emission spectra. Beyond a certain level of the plasma density, the ion-acoustic waves are damped (or Landau damping) by the interaction with the effective number of the plasma ions present in the source plasma. The interaction between the ion-acoustic wave with the ion particles happensbecause the ion-acoustic phase velocity falls in the comparable range of the thermal ion velocity.

The authors would like to support their arugument about the ion deceleration by “Landau damping” like electrons indirectly through their findings of the fine structure in the frequency spectrum. The observed spectrum with fine structures contains useful information on the power absorption by the plasma through different routes. The fine frequency spectra representing the ion plasma wave are explained by estimating the electron energy distribution functions of the Langmuir probes placed in the highly inhomogeneous plasma source. It is found that the ion plasma waves are falling in the ion-acoustic frequency range and their energy transfer to the ions perturbs the electron’s distribution function across a wide electron temperature range in the plasma. The conclusion on the ion’s contribution to the ion-acoustic wave damping is drawn from the ion thermal velocity estimation, deduced from the measured ion-acoustic wave frequency and its wave vector values, electron temperature, etc.Therefore, a direct measurement of the ion temperature to validate the argument is necessary and requires further investigation.

References

[1] Hasegawa Y *et al* 2017 *Jpn. J. Appl. Phys.* **56** 046203

[2] Hotta M *et al* 2017 *Jpn. J. Appl. Phys.* **56** 116002

[3] Zhang Lin and Ouyang Ji-Ting 2016 *J. Phys. D: Appl. Phys.***49** 195105

[4] Gammino S et al., *Rev. Sci. Instrum.* 2010 **81** 02B313

[5] Hofmann I and Boine-Frankenheim O., *Phys. Rev. Accel. Beams* 2017 **20** 014202

[6] Babu P.S and Naik V., 2019 *Phys. Plasmas***26** 033101

[7] Naselli E et al., 2019 *Plasma Sources Sci. Technol.***28** 085021

[8] Mallick C., Bandyopadhyay M. and Kumar R., 2019 *Phys. Plasmas***26** 043507

[9] Mallick C., Bandyopadhyay M. and Kumar R., 2018 *Rev. Sci. Instrum.***89** 125112

[10] Hansen S. K. *et al* 2017 *Plasma Phys. Control. Fusion* **59** 105006

[11] Cortázar O. D., Megía-Macías A. and Tarvainen O., 2014 *Plasma Sources Sci. Technol.* **23**065028

[12] Castro G. etal2017Plasma Sources Sci. Technol. **26** 055019

[13] Oosako T. *et al* 2009 *Nucl. Fusion* **49** 065020

[14] Grek B. and Porkolab M., 1973 *Phys. Rev. Lett.***30** 836

[15] Moisan M. and Nowakowska H., 2015 *J. Phys. D: Appl. Phys.* **48** 455201

[16] Castro G. et al., 2019 *Rev. Sci. Instrum.***90** 023301

[17] Girka V. O. et al 2015 *Phys.Scr.***90** 065605

[18] Ganguli A et al 1999 *Plasma Sources Sci. Technol.***8** 519

[19] Zhang L and Ouyang Ji-Ting 2016 *J. Phys. D: Appl. Phys.***49** 195105

[20] Girka, I.A. and Kovtun, P.K. 1998 *Tech. Phys.***43**: 1424

[21] GAPONOV A. V and MILLER M.A, 1958 *J. Exptl. Theoret. Phys.* (U.S.S.R.) **34**, 751-752

[22] ASKAR'YAN G. A et al. 1962 *J. Exptl. Theoret. Phys. (U.S.S.R.)***42** 1360-136

[23] Celona L et al., 2011*Eur. Phys. J. D.* **61**107-115

[24] Tarvainen O et al., 2016Rev. Sci. Instrum. **87**093301

[25] Khalil Sh. M and Mousa N.M, 2014 *J. Theor. Appl. Phys.***8** 111

[26] www.comsol.com,*COMSOLMultiphysics Reference Manual*, version 5.2, COMSOL, Inc.

[27] Aliev Y M et al., 1992 *Plasma Sources Sci. Technol.***1**126-131

[28] Köhn A et al., 2008 Plasma Phys. Control. Fusion **50** 085018

[29] Mascali D. et al, 2013 *Plasma Sources Sci. Technol.***22** 065006

[30] Podoba Y.Y et al, 2007 *Phys. Rev. Lett.*98 255003

[31] Bernhardt P.A. *et al*2009 *Ann. Geophys.***27** 4409–4427

[32] Fischer P. *et al* 1987 *Journal de Physique* **48** 233-238

[33] Bychenkov V. Y et al., Phys. Rev. E, 6759-6775, **52**, 1995

[34]Moisan M. and Leprince P., 1975 *BeiträgePlasmaphysik***15** 83–104

[35] Cassedy E. S and Mulser P., 1974 *Phys. Rev. A***10** 2349

[36] Mallick C. et al., 2016 *Proceedings of ECRIS2016*, ISBN: 978-3-95450-186-1

[37] Suryanarayana N.S., Kaur J. and Dubey V., 2010 *J. Mod. Phys.***1** 281-289

[38] Watanabe S and Tanaca H., 1973 *Plasma Phys.***15** 501